Blue Sky Catastrophe in Double-Diffusive Convection

Esteban Meca,* Isabel Mercader, Oriol Batiste, and Laureano Ramírez-Piscina

Departament de Física Aplicada, Universitat Politècnica de Catalunya, Jordi Girona 1-3, E-08034 Barcelona, Spain

(Received 10 September 2003; published 11 June 2004; publisher error corrected 15 June 2004)

A global bifurcation of the blue sky catastrophe type has been found in a small Prandtl number binary mixture contained in a laterally heated cavity. The system has been studied numerically applying the tools of bifurcation theory. The catastrophe corresponds to the destruction of an orbit which, for a large range of Rayleigh numbers, is the only stable solution. This orbit is born in a global saddle-loop bifurcation and becomes chaotic in a period-doubling cascade just before its disappearance at the blue sky catastrophe.

DOI: 10.1103/PhysRevLett.92.234501 PACS numbers: 47.27.Te, 47.20.Ky, 44.25.+f

Bifurcation theory has long been a very helpful tool in the analysis of complex dynamics of nonlinear systems [1,2]. Whereas different devised scenarios have been found in theoretical models with a few variables, there is a growing interest both in relating real systems with those kinds of models (e.g., projecting their dynamics to some relevant degrees of freedom [3]) and in directly analyzing the behavior of these systems in terms of dynamical systems theory (by studying them either experimentally or by realistic models). In this context a great deal of work has been devoted to convection in fluids. Qualitative changes in the dynamics of fluxes maintained out of equilibrium by imposed thermal gradients have provided examples of most of the known bifurcations, and have become a main subject in the area of nonlinear dynamics.

In this Letter we will show the occurrence of a blue sky catastrophe (BSC) in double-diffusive convection. The BSC is a codimension-1 bifurcation that consists in the destruction of a stable periodic orbit as its length and period tend to infinity, while the cycle remains bounded and located at a finite distance from all the equilibrium solutions [1,4]. This destruction is caused by the collision with a nonhyperbolic cycle that appears at the bifurcation point. While approaching the bifurcation the orbit increasingly coils in the zone where the new cycle will appear, which originates the divergence in both period and length. In that point the original cycle becomes an orbit homoclinic to the new cycle. This type of bifurcation is relatively exotic, but can easily be found in slow-fast (i.e., singularly perturbed) systems with at least two fast variables [5].

We are interested in double-diffusive fluxes that occur when convection is driven by simultaneous thermal and concentration gradients in a binary mixture [6]. Double-diffusive convection in cavities with imposed vertical gradients exhibits very rich dynamics, and has been used as a system to study pattern formation [7] and transition to chaos [8]. The case of horizontal gradients, which arises naturally in applications such as crystal growth [9] or oceanography [6], has received less attention. In this work we numerically study this latter configuration for a small Prandtl number binary mixture. We consider the case when thermal and solutal buoyancy forces exactly compensate each other, which allows the existence of a quiescent (conductive) state [10–13]. We have found that in this system there exists a large range of Rayleigh numbers in which the only stable solution is an orbit that features a low-frequency spiking behavior. This orbit appears associated to a global bifurcation and loses stability when a period-doubling cascade takes place originating a chaotic attractor. However, the most remarkable feature of this chaotic attractor is its sudden disappearance in a BSC of the chaotic type. As far as we know this is the first example of such bifurcation in an extended system.

We have considered a binary mixture in a 2D rectangular cavity of aspect ratio $\Gamma = d/h = 2$, where d is the length and h is the height of the cavity. A difference of temperature ΔT is maintained between both vertical boundaries. Dimensionless equations in Boussinesq approximation explicitly read

$$\partial_t \mathbf{u} + (\mathbf{u}\cdot\nabla)\mathbf{u} = -\nabla P + \sigma\nabla^2\mathbf{u} + \sigma \mathrm{Ra}[(1+S)(-0.5 + x/\Gamma) + \theta + SC]\hat{\mathbf{z}}, \quad (1)$$

$$\partial_t \theta + (\mathbf{u}\cdot\nabla)\theta = -v_x/\Gamma + \nabla^2\theta, \quad (2)$$

$$\partial_t C + (\mathbf{u}\cdot\nabla)C = -v_x/\Gamma - \tau\nabla^2(\theta - C), \quad (3)$$

$$\nabla\cdot\mathbf{u} = 0, \quad (4)$$

where $\mathbf{u} \equiv (v_x, v_z)$ is the velocity field in (x, z) coordinates, P is the pressure over the density, θ denotes the departure of the temperature from a linear horizontal profile. C is the scaled deviation of the concentration of the heavier component relative to the linear horizontal profile which equilibrates that of the temperature in the expression of the mass flux. Lengths and times are scaled with h and $t_\kappa = h^2/\kappa$, respectively, with κ being the thermal diffusivity. The dimensionless parameters are

the Prandtl number $\sigma = \nu/\kappa$, the Rayleigh number $\mathrm{Ra} = \alpha g h^3 \Delta T/\nu\kappa$, and the Lewis number $\tau = D/\kappa$, where ν denotes the kinematic viscosity, g the gravity level, α the thermal expansion coefficient, and D is the mass diffusivity. The separation ratio $S = C_0(1 - C_0)\frac{\beta}{\alpha} S_T$ will be taken $S = -1$. Here, S_T is the Soret coefficient, C_0 is the concentration of the heavier component in the homogeneous mixture, and β is the mass expansion coefficient ($\beta > 0$ for the heavier component).

The boundaries are taken to be no-slip and with no mass flux. Lateral walls are maintained at constant temperatures and at the horizontal plates a linear profile of temperature between the two prescribed temperatures is imposed. Thus, boundary conditions are written as

$$\mathbf{u} = \theta = \mathbf{n} \cdot \nabla(C - \theta) = 0, \quad \text{at } \partial\Omega. \tag{5}$$

Notice that these boundary conditions prevent one from absorbing the Soret terms into the equations as in Refs. [10–13]. On the other hand, this system is $\mathbb{Z}_2$ equivariant. Equations (1)–(4), together with boundary conditions (5), are invariant under a transformation π, a central symmetry around the point $(\Gamma/2, 1/2)$, i.e., π: $(v_x, v_z, \theta, C) \to (-v_x, -v_z, -\theta, -C)$, $(x, z) \to (\Gamma - x, 1 - z)$. Hence any solution of these equations either is π invariant (from now on we will call it symmetric) or its image under π is also a solution (constituting a pair of asymmetric solutions). This has important consequences on the nature of its possible bifurcations [1].

We have obtained time-dependent solutions of Eqs. (1)–(4) and boundary conditions (5) by using a second order time-splitting algorithm, proposed in Ref. [14], and a pseudospectral Chebyshev method for the space discretization. Furthermore, we have calculated (both stable and unstable) steady solutions and analyzed their stability by adapting a pseudospectral first-order time-stepping formulation, as described in Refs. [15,16,17]. The values of the parameters have been $\sigma = 0.00715$ and $\tau = 0.03$, close to that characteristic of molten doped germanium [18,19]. Spatial discretization has typically been between 60×30 and 90×60 mesh grid points.

The scenario provided by the analysis of the steady solutions is shown in the bifurcations diagram of Fig. 1. In this figure the Nusselt number, defined as the quotient of heat flux through the hot wall with that of the corresponding conductive solution, is represented for the steady states as a function of the Rayleigh number (Ra). For the sake of clarity only one asymmetric solution of each pair has been shown. For small Ra the conductive solution (allowed here by the choice $S = -1$) is stable, but loses stability, maintaining the symmetry, through a transcritical bifurcation at $\mathrm{Ra} = 541.9$. The supercritical branch of the bifurcating solution is stable only up to a pitchfork bifurcation at $\mathrm{Ra} = 542.4$, following a scenario similar to that described in Ref. [12]. The interesting behavior in this system originates from the subcritical branch. This branch gains stability via a saddle-node bifurcation at

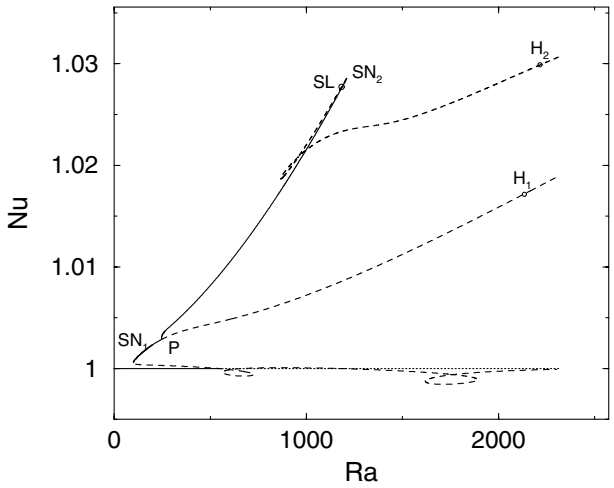

FIG. 1. Nusselt number of steady solutions versus Ra, and its corresponding bifurcations. Continuous lines: stable states. Dashed lines: unstable states.

$\mathrm{Ra} = 99$ (SN_1), and loses it again at $\mathrm{Ra} = 245$ in a Pitchfork bifurcation (P) where a couple of stable asymmetric branches appear. In Fig. 2 we represent the concentration for symmetric (left) and asymmetric (right) steady states. We can see that concentration is roughly homogeneous inside rolls, displacing concentration gradients to the lateral boundaries.

The asymmetrical steady state is stable until $\mathrm{Ra} = 1209$, where it loses stability at a saddle-node bifurcation (SN_2). The full branch of asymmetrical steady states is depicted in Fig. 1, where we can see that it changes again the direction at a turning point at $\mathrm{Ra} = 865.6$, but without gaining stability. Increasing the Rayleigh number Hopf bifurcations of the symmetric and asymmetric branches take place at H_1 ($\mathrm{Ra} = 2137$) and H_2 ($\mathrm{Ra} = 2218$), respectively. The branch of symmetric periodic orbits emanating from H_1 will play an essential role in the subsequent evolution of the system.

In the range from $\mathrm{Ra} = 1209$ until $\mathrm{Ra} = 2253$ we have found no stable solution connected with the above branches by local bifurcations. Integrating the evolution equations we have obtained a branch of asymmetric periodic solutions that dominates the dynamics of the system in this range of parameters. In Fig. 3 we represent time series and phase space plots of the orbits of this branch for two different values of the Rayleigh number. The oscillations first appear in the form of spikes of very large

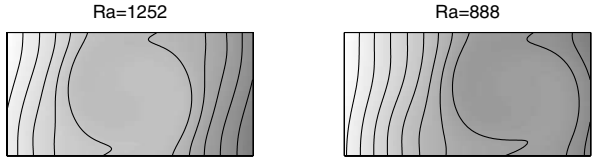

FIG. 2. Concentration levels of the steady solutions of the symmetric branch ($\mathrm{Ra} = 1252$) and the nonsymmetric branch ($\mathrm{Ra} = 888$).

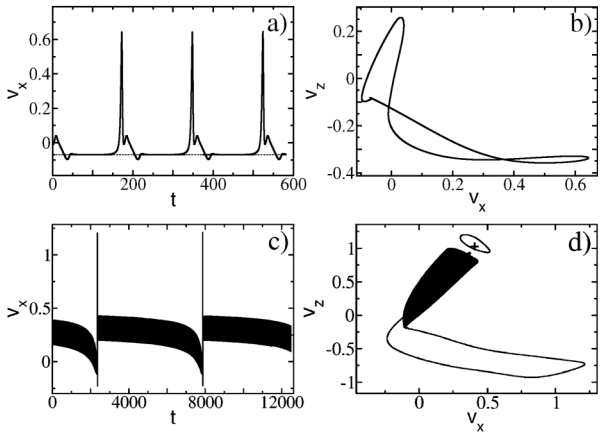

FIG. 3. Velocity components of a representative point. Top: Asymmetric orbit at Ra = 1183.68. (a) time series, with the value of the saddle stationary solution marked. (b) orbit in the phase space. Bottom: Attractor at Ra = 2255. (c) time series. (d) attractor in the phase space with the stable symmetric orbit. The unstable stationary symmetric solution is also shown.

period [see Fig. 3(a)], according to the proximity to a global saddle-loop (SL) bifurcation that occurs at Ra = 1183.67 (SL) where the orbit connects with the unstable branch of SN_2 (see Fig. 1). The character of this global bifurcation can be inferred from the logarithmic divergence of the period when the Rayleigh number decreases toward SL. We have fitted that period to

$$T \sim -\frac{1}{\lambda}\log(\mathrm{Ra} - \mathrm{Ra}_{\mathrm{SL}}) + A. \tag{6}$$

We can see the fit in Fig. 4 (left). The resulting value $\lambda_{\mathrm{fit}} = 0.079$ results in being quite close to the unstable eigenvalue $\lambda = 0.074$ of the saddle stationary point, as obtained by the stability calculation. Near that global bifurcation the time evolution of the velocity of a representative point is shown in Fig. 3(a). The value for the saddle asymmetric state is also represented. We can see how the solution spends a long time near it. The spike corresponds to a rapid and large excursion by the phase space, as seen in Fig. 3(b), during which the roll alternately switches between a confined and a more centered position (analogous to the patterns shown in Fig. 2).

Increasing Ra, at Ra = 2137 the orbit starts to curl, showing ripples in the time dependence, reflecting the frequency of the unstable symmetric orbit that appears in H_1. In fact, we have been able to calculate this unstable branch by temporal evolution forcing the symmetry of the system, and its frequency coincides with that of the windings of the attractor on all the branch. If we increase further Ra, the asymmetric orbit follows a period-doubling cascade, becoming chaotic. This is revealed in the phase of the winding of the trajectory, as can be seen in Fig. 5 where a detail of the orbit during the cascade is shown. This cascade seems to move to slightly higher Ra values as spatial resolution is increased, but we have not been able to obtain the precise values due to the extremely large duration of the orbits in this regime. In Fig. 3(c) and

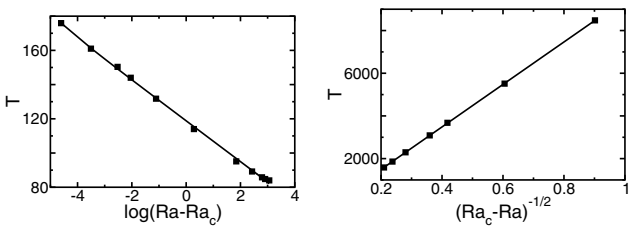

FIG. 4. Left: logarithmic fit of the periods for the SL connection. Right: Square-root fit of the periods for the BSC.

3(d) the attractor thus generated is represented at Ra = 2255. For this value of Ra the symmetric orbit has already become stable at a Pitchfork bifurcation (P_{so}, at Ra = 2253), and both coexist. Very shortly afterwards, the whole attractor disappears at Ra = 2257.5.

This destruction of the attractor exhibits characteristics that permit one to identify it as the chaotic counterpart of the scenario for BSC bifurcation described in Refs. [1,20]. Indeed in all the process the attractor remains bounded and at a finite distance of any steady solution, as required [1]. The average length and time between spikes (which are reproducible with variations smaller than 1 over 1000) diverges as the windings start to accumulate, which occurs at a specific location in the attractor. That indicates that the solution is colliding there with a new cycle that appears at the bifurcation point, and to which it becomes homoclinic. Furthermore this divergence, shown in Fig. 4 (right), is very well fitted by a square-root law:

$$T \sim \frac{A}{\sqrt{\mathrm{Ra}_c - \mathrm{Ra}}} + B. \tag{7}$$

This law of divergence particularly corresponds to that scenario, since it demonstrates that the new cycle to which the attractor is connecting is the saddle node of two orbits (SNO_1). In principle there are several possibilities for the topology of the attractor [4]. In our case the

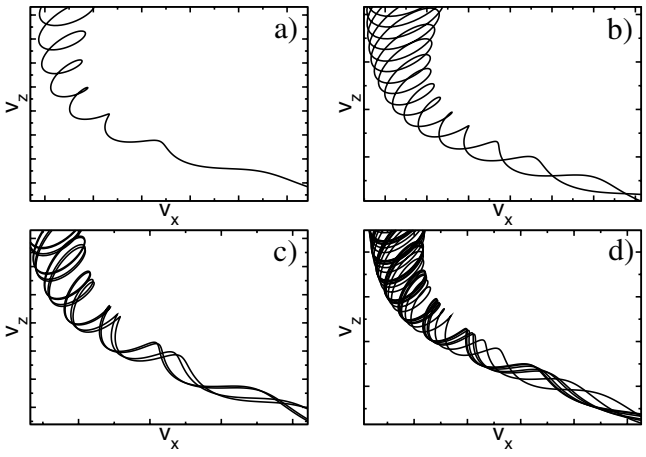

FIG. 5. Period-doubling cascade (zoom of the tip of the attractor). (a) period 1 (Ra = 2220). (b) period 2 (Ra = 2232). (c) period 4 (Ra = 2235). (d) chaotic solution (Ra = 2240).

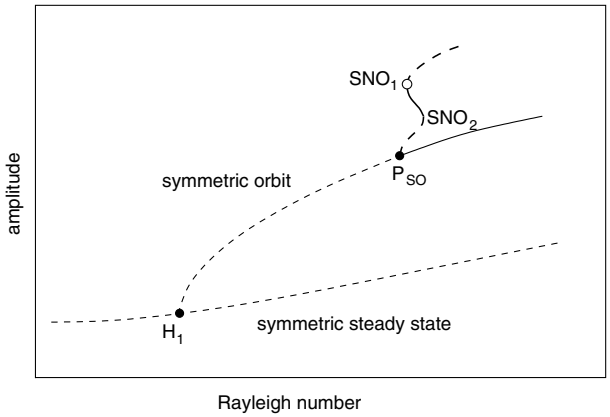

FIG. 6. Diagram of the conjectured unstable asymmetric orbit (thick line) and its connections to other branches.

successive windings are braided by the tip of the attractor into an almost one dimensional tube or filament (Fig. 5). This filament reintroduces the orbit into the vicinity of the saddle-node orbit, and it starts winding again accumulating curls near it. Therefore, in the limit, the attractor has the topology of a French horn. This feature is also shared with Ref. [20].

After the BSC, one would expect the system to reach the stable member of the pair of asymmetric solutions born at SNO_1. On the contrary, simulations show that the system evolves through an extremely long transient, during which the trajectory accumulates curls near the saddle node before being rejected to the symmetric orbit that became stable at P_{SO}. That could mean either that the stability range of the asymmetric orbit is very small (which would require a much finer exploration in Ra to find it, a formidable task in this slow regime), or that its basin of attraction is very reduced (and the nearby symmetric orbit attracted all the calculated orbits).

We propose that the SNO_1 is located in the branch of unstable asymmetric orbits created at the pitchfork bifurcation where the new orbit becomes stable (P_{so}). This hypothetical scenario is shown in Fig. 6, and is the simplest one in which the attractor presents at the BSC a homoclinic connection to a branch coming from known solutions. This conjecture requires the unstable asymmetric branch to gain stability in a first saddle-node bifurcation SNO_2 and to lose it again at the SNO_1, as can be seen in Fig. 6. The coincidence of the frequency value of the symmetric orbit at P_{SO}, $\omega_{SO} = 7.01$, to that of the windings of the attractor, $\omega = 7.01$, is consistent with such a connection. A small distance between SNO_1 and SNO_2 would explain the reduced stability domain of the asymmetrical solution. Finally, the presence of the additional saddle-node orbit SNO_2 in the proximity would slow down the dynamics for Ra slightly above, making the transient to the symmetric solution very long, as it is actually observed.

One could devise more complex scenarios for the occurrence of this BSC. For example, the attractor could be destroyed on a boundary crisis associated to global connections of the unstable orbits coming from the period-doubling bifurcations.

Finally, it is worth remarking than the BSC displayed by this system is robust against small changes in the value of the separation ratio S. In particular, we have obtained a similar BSC in simulations performed with $S = -0.99$. That means that the additional symmetry introduced in the system by the special value $S = -1$ is not an essential ingredient of the phenomena described here.

This work was financially supported by Dirección General de Investigación Científica y Técnica (Spain) (Projects No. BFM2003-00657 and No. BFM2003-07850-C03-02) and Comissionat per a Universitats i Recerca (Spain) Projects No. 2001/SGR/00221 and No. 2002/XT/00010. We also acknowledge computing support from CEPBA (Spain). E. M. acknowledges a grant from Ministerio de Educación, Cultura y Deporte (Spain).

*Electronic address: esteban@fa.upc.es

[1] Y. Kuznetsov, *Elements of Applied Bifurcation Theory*, Applied Mathematical Sciences Vol. 112 (Springer-Verlag, New York, 1998), 2nd ed.
[2] J. Guckenheimer and P. Holmes, *Nonlinear Oscillations, Dynamical Systems, and Bifurcations of Vector Fields, of Applied Mathematical Sciences* (Springer-Verlag, New York, 1983), Vol. 42.
[3] J. Bhattacharjee, *Convection and Chaos in Fluids* (World Scientific, Singapore, 1987).
[4] L. Shilnikov and D. Turaev, Am. Math. Soc. Transl. **200**, 165 (2000).
[5] A. Shilnikov, L. Shilnikov, and D. Turaev Moscow Math. J. (to be published).
[6] J. Turner, Annu. Rev. Fluid Mech. **17**, 11 (1985).
[7] M. Cross and P. Hohenberg, Rev. Mod. Phys. **65**, 851 (1993).
[8] E. Knobloch, D. Moore, J. Toomre, and N. Weiss, J. Fluid Mech. **166**, 409 (1986).
[9] J. Turner, Nature (London) **285**, 213 (1980).
[10] K. Ghorayeb and A. Mojtabi, Phys. Fluids **9**, 2339 (1997).
[11] S. Xin, P. L. Quéré, and L. Tuckerman, Phys. Fluids **10**, 850 (1997).
[12] G. Bardan, A. Bergeon, E. Knobloch, and A. Mojtabi, Physica (Amsterdam) **138D**, 91 (2000).
[13] A. Bergeon and E. Knobloch, Phys. Fluids **14**, 3233 (2002).
[14] S. Hugues and A. Randiamampianina, Int. J. Numer. Methods Fluids **28**, 501 (1998).
[15] C. Mamun and L. Tuckerman, Phys. Fluids **7**, 80 (1995).
[16] A. Bergeon, D. Henry, H. Benhadid, and L. Tuckerman, J. Fluid Mech. **375**, 143 (1998).
[17] S. Xin and P. L. Quéré, Phys. Fluids **13**, 2529 (2001).
[18] D. H. Kim, P. M. Adornato, and R. A. Brown, J. Cryst. Growth **89**, 339 (1988).
[19] P. M. Adornato and R. A. Brown, J. Cryst. Growth **80**, 155 (1987).
[20] L. Shilnikov, Int. J. Bifurcation Chaos Appl. Sci. Eng. **7**, 1953 (1997).